

# Ultralow-voltage field-ionization discharge on whiskered silicon nanowires for gas-sensing applications

Ramin Banan Sadeghian and M. Saif Islam\*

**Several hundred million volts per centimetre of electric-field strength are required to field-ionize gas species. Such fields are produced on sharp metallic tips under a bias of a few kilovolts. Here, we show that field ionization is possible at dramatically lower fields on semiconductor nanomaterials containing surface states, particularly with metal-catalysed whiskers grown on silicon nanowires. The low-voltage field-ionization phenomena observed here cannot be explained solely on the basis of the large field-amplification effect of suspended gold nanoparticles present on the whisker tips. We postulate that field penetration causes upward band-bending at the surface of exposed silicon containing surface states in the vicinity of the catalyst. Band-bending enables the valence electron to tunnel into the surface states at reduced fields. This work provides a basis for development of low-voltage ionization sensors. Although demonstrated on silicon, low-voltage field ionization can be detected on any sharp semiconductor tip containing proper surface states.**

Development of devices that can field-ionize gas molecules at low bias voltages may be essential for many applications such as ion mobility spectrometry<sup>1</sup> and highly selective portable gas sensing. Recent developments in synthesis of dense nanostructures with ultrasharp tips offered promise to ionize gas molecules for their accurate fingerprinting, but their high operating voltages are not favourable for ubiquitous applications<sup>2–4</sup>.

Field ionization (FI) consists of a valence electron of a gas atom or molecule (henceforth referred to as a particle) tunnelling through a potential barrier, commonly into a vacant energy state of the conduction band of a metal at the anode<sup>5</sup>. Classic FI action on metallic specimens requires extremely high positive electric fields, of the order of a few hundred million volts per centimetre. Such fields are only achievable in the vicinity of very sharp electrodes under a large bias. For instance, to produce FI of nitrogen on metal tips with end radii of  $r_t \approx 10\text{--}20\text{ nm}$ , it is necessary to apply a bias of 1–2 kV (ref. 6). Figure 1a shows the potential diagram of an imaging particle near a metal surface subject to a positive field. There is a critical distance ( $d_c$ ) between the particle and the metal surface below which FI cannot occur.  $d_c$  is about 4–5 Å for metals and is given by

$$d_c \cong (U_1 - \Phi)/eF_{\text{vac}} \quad (1)$$

where  $U_1$  is the ionization potential of the particle,  $\Phi$  is the metal work function,  $e$  is the elemental electron charge and  $F_{\text{vac}}$  stands for the electric field in vacuum at the metal surface. Figure 1b shows a three-dimensional schematic view of a single nanowire bearing whiskers branching from the trunk. Each whisker can act as an individual FI source, because at the apex it carries the highest electric field among other prominent features. Figure 1c shows a magnified view of a generic FI tip that can be the apex of one of the whiskers. A comprehensive illustration of various particle–tip interactions is presented in this figure at the atomic scale. Particles can be supplied from the surroundings or crawl up along the specimen shank to the ionization zone. The former process dominates at low

fields and the latter at low temperatures or at high fields where the current is limited by gas supply<sup>7</sup>. Considerably higher field strengths are necessary to ionize a particle adsorbed on a prominent surface atom than one in the gas phase several ångströms away from it. Ionization of an adsorbed particle is referred to as field desorption, or field evaporation if the particle originates from the specimen lattice itself.

Here we show that FI can take place at dramatically lower field strengths, at the surface of sharp semiconductor–metal interfaces containing surface states. Occurrence of exotic ionization discharge on gold-catalysed whiskered silicon nanowires was demonstrated. In particular, measurable FI currents were recorded at below 10 V, that is, three orders of magnitude smaller than the voltages recorded using sharp metallic specimens<sup>6</sup>. In addition to the lowering of threshold FI voltages, we showed that whiskering at the nanoscale provides an ample number of FI sites, so that, even though each whisker has an extremely small contribution, the total field-ion current can be detectable.

## Detection of anomalous FI

Silicon nanowires covered with dense whiskers were grown using a two-step vapour–liquid–solid (VLS) technique<sup>8</sup> (see Methods). Measurements were carried out on as-grown whiskered nanowires, whiskered nanowires after removal of gold tips, and regular whiskerless nanowires. The effect of doping on the FI current was studied as well. Scanning electron microscopy (SEM) micrographs of the smooth and whiskered silicon(111) nanowires are shown in Fig. 2a and b–d respectively. The nanowires were incorporated at the anode of identical ionization cells with an electrode separation of 100  $\mu\text{m}$  (Fig. 2e). Thus, a bias of  $V = 10\text{ V}$  would produce an applied field of  $10^3\text{ V cm}^{-1}$ . Such a field must be amplified by a factor of  $\sim 1.7 \times 10^5$  to generate  $1.7 \times 10^8\text{ V cm}^{-1}$  (this is the best-image field of  $\text{N}_2$ ; the threshold field strength might be slightly smaller), required to field-ionize nitrogen on metallic tips<sup>6,9</sup>. Various models have been proposed to explain

Department of Electrical and Computer Engineering, University of California—Davis, 2064 Kemper Hall, Davis, California 95616-5294, USA.

\*e-mail: sislam@ucdavis.edu.

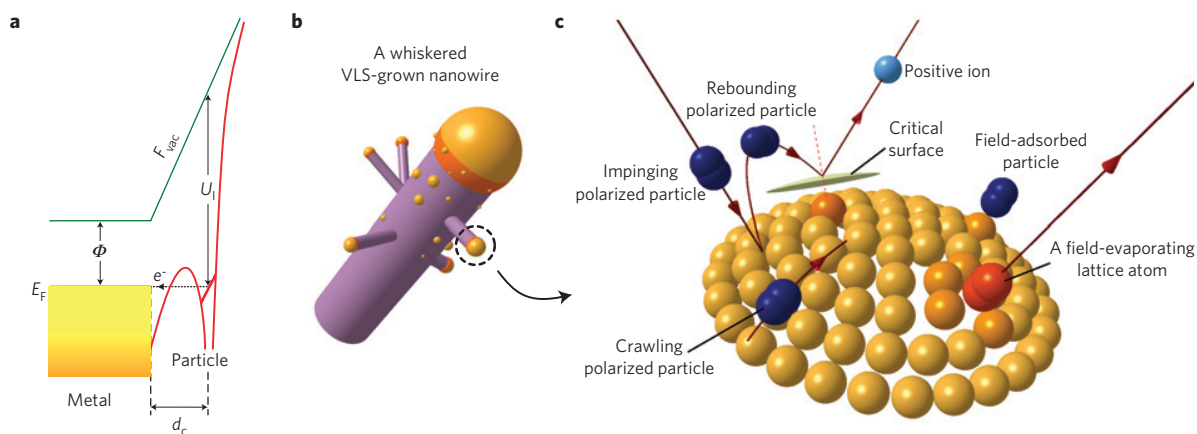


**Figure 1 | Field ionization dynamics.** **a**, Energy-band diagram for FI of a gas particle under a positive applied field in the vicinity of a metal surface.  $E_F$  is the Fermi level,  $\Phi$  is the metal work function,  $U_I$  is the ionization potential,  $F_{vac}$  is the electric-field strength in vacuum and  $d_c$  is the distance at which  $E_F$  and the ground state of the atom coincide, referred to as the critical distance. **b**, Schematic illustration of a VLS-grown nanowire containing whiskers on the trunk. **c**, Atomic-scale view of a sharp tip that can be the apex of one of the nanoscale whiskers, showing field ionization and field adsorption of an alien particle (double lobe dark, or blue in the coloured version), and field evaporation of a lattice atom (double lobe light, or orange in the coloured version). The lattice atoms (spheres) are drawn without taking into account any specific crystal orientation. FI can happen after the impinging particle loses its kinetic energy during several rebounds, or, at higher fields, the particle crawls up to the specimen trunk up to the ionization zone. The latter process is referred to as field desorption. The critical distance,  $d_c$ , is depicted as a 'critical surface' (disc) in the three-dimensional illustration.

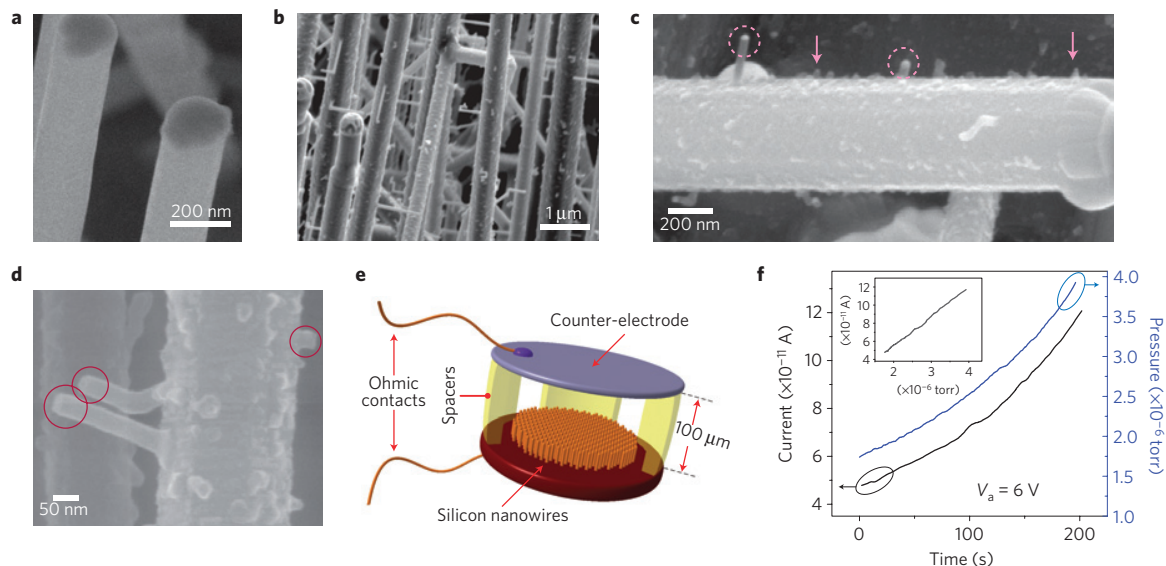


**Figure 2 | Nanowires used to measure anomalous semiconductor-assisted gas ionization.** **a**, A close-up SEM image of smooth silicon nanowires after annealing in HCl. **b, c**, SEM micrographs of a forest of, and a single, whiskered silicon nanowire that showed low-voltage FI; **d**, that of whiskered nanowires after removal of gold catalyst for the tips. **e**, A three-dimensional schematic illustration of the device used to measure gas ionization on both types of nanowire. Note that the nanowires were planted at the anode.  $d_{gap} = 100 \mu\text{m}$  is the spacing between anode and cathode. **f**, The anode discharge current in  $\text{N}_2$ , and the  $\text{N}_2$  pressure, versus time at  $V = 6 \text{ V}$ . The curves were obtained using the device with undoped whiskered silicon nanowires. As the current-versus-pressure curve in the inset shows, the discharge current is proportional to the gas pressure, which is evidence of FI being the dominant conduction process.

the field-enhancement effect on sharp tips<sup>10–12</sup>, but owing to the vast variety of shape and size of the whiskers, ranging from well-protruded branches to small buds, it is impossible to define a single enhancement factor for the apparatus (see Supplementary Information). Nevertheless, even the sharpest whiskers formed on our silicon nanowires are not capable of producing such high field-amplification factors. The upper limit of the field strength at the apex of a hemisphere-on-shank is given by  $F_{max} \approx V/5r_t$  (ref. 5). As a result, to achieve  $1 \text{ V } \text{\AA}^{-1}$  ( $10^8 \text{ V cm}^{-1}$ ), at  $V = 10 \text{ V}$ , the protrusion tip curvature needs to be about  $r_t \approx 2 \text{ \AA}$  (0.2 nm),

obviously far sharper than the whisker tips grown in this work. Figure 2f shows the evolution of discharge current with time, measured while nitrogen was slowly injected into the test chamber. The curve was obtained using the device containing undoped whiskered nanowires with their gold catalyst intact. Interestingly, the linear dependence of current on pressure is consistent with FI action. The other two nanowire variants did not show FI within the voltage range studied. Figure 3a shows the  $I$ - $V$  curves of undoped whiskered nanowires obtained in a wide pressure range of nitrogen in full logarithmic coordinates. The inset shows the pressure

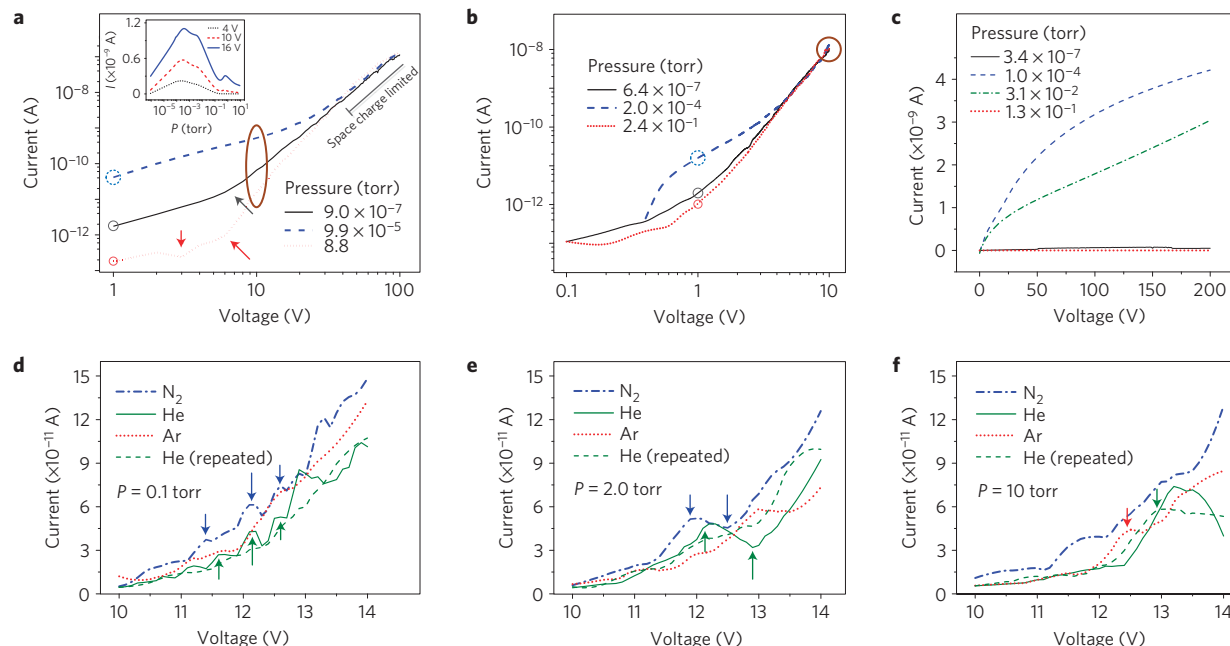


**Figure 3 | Current-voltage curves.** **a, b**,  $I$ - $V$  characteristics of  $N_2$  discharge obtained in a wide pressure range using undoped (**a**) and p-type doped (**b**) whiskered nanowires plotted in log-log coordinates. **c**,  $I$ - $V$  curves obtained from undoped whiskered nanowires after the gold catalyst was etched from the tips. No FI action was detected. **d-f**,  $I$ - $V$  curves corresponding to field desorption of nitrogen, helium and argon at  $P = 0.1$ , 2 and 10 torr respectively measured using undoped whiskered nanowires. The relative amplitudes of currents indirectly match the relative ionization potentials of the species, as helium with the highest  $U_1$  shows the lowest current. The coupled arrows indicate voltages at which desorption sites with similar bonding energies are activated in the process of desorption of nitrogen and helium in cases **d** and **e**, and desorption of argon and helium in **f**.

dependence of current at three bias voltages. In contrast to the case of discharge in parallel plates, where the conduction is ohmic at low voltages, conduction begins with FI at  $1 \lesssim V \lesssim 6$  V. Note the slightly greater-than-unity slopes in this region, particularly at low pressure. At low fields, the FI current is expected to rigorously depend on the field strength (field-limited regime) and to be a strong function of  $U_1$  (refs 5,7). Such dependence can be employed to fingerprint the unknown gas particle, as  $U_1$  is a unique quantity. However, no tangible difference was observed between the  $I$ - $V$  curves of nitrogen, helium, argon and ammonia, particularly at  $V \lesssim 6$  V. We therefore conclude that  $V \lesssim 6$  V corresponds to the supply-limited regime, where the ionization rate is already high enough that all of the impinging particles are ionized and the current mildly increases with field strength. The supply-limited FI current does not depend on  $U_1$ , whereas it is proportional to the gas pressure close to the tip. The steep current rise observed at  $V \simeq 6$  V can be associated with desorption of field-adsorbed particles along the nanowires, which owing to polarization forces crawl up to the apex of whiskers, where the field strength is maximum. At high voltages the curves converge, for the conduction becomes space charge limited. In this regime, the space-charge-limited insulator injected plasma cube law holds because the curves have a slope of  $\sim 3$ , that is,  $I \propto V^3$  (ref. 13). The  $I$ - $V$  curves obtained from the p-type doped whiskered nanowires are shown in Fig. 3b. At low voltages, where we believe FI begins, the amplitudes of the probed currents are comparable to that of the undoped sample. This is suggestive that FI is not a strong function of the Fermi level in the bulk of protrusions. However, the doped sample exhibits larger current at higher voltages, consistent with its lower resistivity. Anomalous FI ceased on whiskered nanowires after removal of the gold catalyst from their tips. Figure 3c shows the resultant  $I$ - $V$  curves, which resemble that of discharge in parallel plates where the conduction is ohmic at low voltages and tends to saturate before the Townsend discharge mechanism takes effect.

### Selectivity in the field-desorption regime

Figure 3d-f shows the  $I$ - $V$  curves corresponding to field desorption of nitrogen, helium and argon, measured using undoped whiskered nanowires at three different pressures ( $P = 0.1$ , 2 and 10 torr respectively). In comparison to the low-pressure scenario, the rate of FI of the desorbing particle decreases owing to formation of a multi-adlayer of gas molecules on the emitter surface. As a result, in contrast to the low-pressure case, where all the species in the gap are ionized ( $P = 10^{-7}$ - $10^{-4}$  torr in Fig. 3a and the inset), the discharge current becomes related to  $U_1$ . The phenomenon is discernible in the  $I$ - $V$  curves plotted in Fig. 3d-f, as, in general, the species with higher  $U_1$  have exhibited lower currents. Apparently, this can enable selective gas discrimination on the basis of the field-ion  $I$ - $V$  behaviour of different gas types. It is clearly seen that helium has generated a smaller field-ion current than nitrogen. In addition, activation and deactivation of adsorption sites with different bonding energies has produced kinks that are readily repeated among different gas types. The peaks correspond to the voltages at which these sites start to lose the adsorbed particles owing to field desorption; therefore, the current ceases to rise until a site with a higher bonding energy is activated (valleys). Because of its higher  $U_1$ , the kinks corresponding to the field-ion current of helium lag in voltage as compared with those of nitrogen in Fig. 3d,e, and with those of argon in Fig. 3f. The fact that currents are pressure independent confirms that the ion current is initiated from adsorbed molecules rather than free molecules in the gap.

### Semiconductors versus metals

It is well known that, under certain conditions, FI requires lower applied fields on semiconductors than on metals. Field penetration into the semiconductor may cause significant upward band bending and make the near-surface region become p-type degenerate<sup>6</sup>. As shown in the energy-band diagram of Fig. 4a, the electron may then

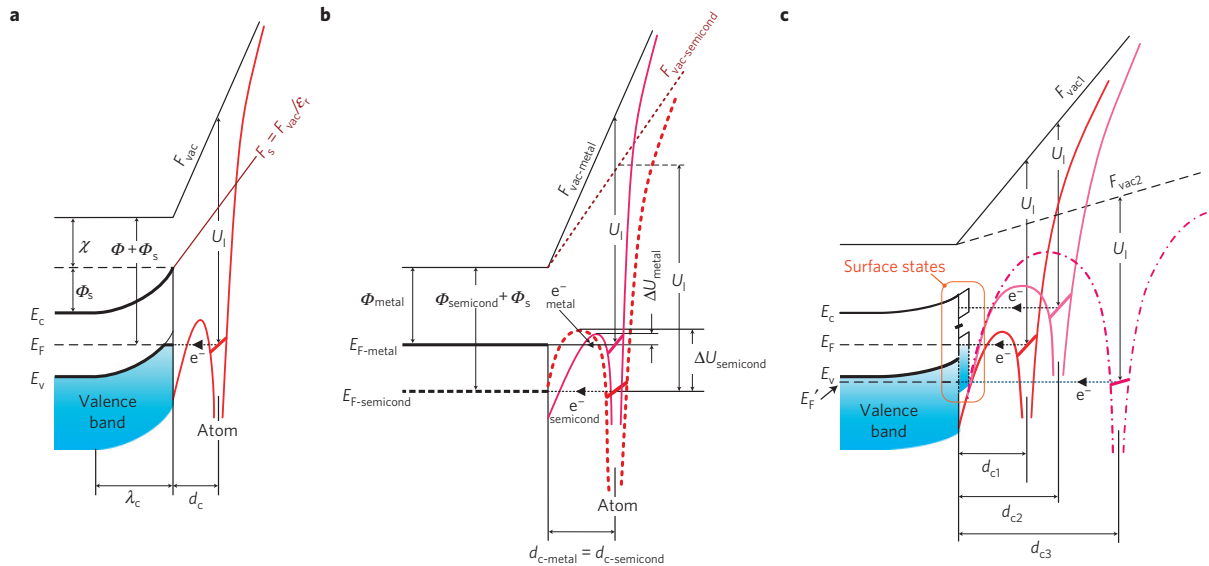


**Figure 4 | Energy-band diagrams for FI on a semiconductor surface.** The semiconductor work function at the surface,  $\Phi$ , increases by the amount of band bending,  $\Phi_s$ , due to field penetration.  $F_{\text{vac}}$  and  $F_s$  are the electric-field strengths in vacuum and semiconductor respectively,  $\lambda_c$  is the field penetration depth and  $\epsilon_r$  is the semiconductor relative permittivity. **a**, This model predicts reduction of  $d_c$  on the semiconductor at the same imaging field owing to a larger effective surface work function. A shorter  $d_c$  implies a higher tunnelling probability and, therefore, a higher field-ion current. **b**, The solid and dotted lines represent the potential energies of the imaging-gas electron near a metal and a semiconductor surface, respectively.  $d_c$  is assumed to be nearly the same for both materials. The potential barrier changes from triangular to trapezoidal, and becomes larger in the semiconductor ( $\Delta U_{\text{semicond}} > \Delta U_{\text{metal}}$ ). As a result, it is expected that the imaging field and the field-ion current decrease at the same time. The effect of surface states is not considered in this model. **c**, The effect of surface states. The tunnelling electron can enter the surface states, even without surface inversion. The tunnelling probability is higher for tunnelling into the states closer to the valence band ( $d_{c1} < d_{c2}$ ). In the low-field case ( $F_{\text{vac}2}$ ), there is normally no empty state available for the ground-state electron to tunnel unless the semiconductor is heavily p-type degenerate. In addition, the penetration probability is very small as  $d_{c3}$  is large.  $E'_F$  is the degenerate Fermi level. The types of surface state that could be involved in the FI process are discussed in detail in Supplementary Information. This last model is more effective in explaining the low-field FI behaviour we observed herein. **c** is not drawn to scale with **a** and **b**.

transfer into the empty states of the valence band above  $E_F$ . The penetration probability is approximately given by

$$D(d_c) \cong \exp(-A\Delta U^{1/2}d_c) \quad (2)$$

where the barrier height is  $\Delta U = U_1 - \Delta V$ , in which  $\Delta V = (e^3 F_{\text{vac}})^{1/2}$ , and  $A$  is a constant<sup>9,14</sup> ( $A = 4/3(2m/\hbar^2)^{1/2}$ , where  $m$  is the free-electron mass, and  $\hbar$  is Planck's constant divided by  $2\pi$ ). The effective work function at the semiconductor surface increases by the amount of band bending, given by

$$\Phi_s = e\lambda(F_{\text{vac}}/\epsilon_r)$$

where  $\epsilon_r$  is the relative permittivity of the semiconductor, and  $\lambda$  is the apparent field penetration depth. According to equation (1), an increase in  $\Phi_s$  can lead to a decrease in  $F_{\text{vac}}$ ,  $d_c$  or both. At fields close to and above the threshold, the field-ion current is rigorously field dependent and proportional to both the gas concentration and the tunnelling probability,  $D$ . Hence, from equation (2) the ratio of the currents in the two cases for a triangular potential barrier becomes

$$\begin{aligned} \frac{I_{\text{semicond}}}{I_{\text{metal}}} &= \frac{D_{\text{semicond}}}{D_{\text{metal}}} \\ &= \exp\left[A\left(d_{c\text{-metal}}\sqrt{\Delta U_{\text{metal}}} - d_{c\text{-semicond}}\sqrt{\Delta U_{\text{semicond}}}\right)\right] \end{aligned} \quad (3)$$

If only  $d_c$  decreases and other parameters, such as  $\Delta V$  (and thus,  $\Delta U$ ), remain unaltered (compare Fig. 4a with Fig. 1a), equation (3) would imply that, at a given field, the field-ion emission current on a semiconductor should be higher because of a smaller  $d_c$  (ref. 14).

The ion currents obtained in this work, however, are not in agreement with (3) for  $d_{c\text{-semicond}} < d_{c\text{-metal}}$ , as their amplitudes are much smaller than if the ion emission were from metallic tips with the same geometry. The total number of FI sites in the sample with whiskered nanowires is estimated to be of the order of  $10^{11}$  from our SEM observations (see Supplementary Information). These are gold-terminated whiskers of silicon with an average tip curvature of roughly  $\bar{r}_t \approx 6.7$  nm. On the occasion of FI at  $V = 6$  V,  $t = 100$  s, where  $I_{\text{FI}} = 7 \times 10^{-11}$  A at  $P = 2.5 \times 10^{-6}$  torr, as shown in Fig. 2f, each whisker is expected to emit a continuous field-ion current of about  $7 \times 10^{-11}$  A/ $10^{11} = 7 \times 10^{-22}$  A, where the upper limit of field strength on the tips would be  $1.8 \times 10^6$  V cm $^{-1}$  at this voltage (using  $F_{\text{max}} = V/5r_t$ ). In fact, this is a rough overestimate: as the whiskers have a certain diameter/length distribution, the local fields could be weaker (see Supplementary Information). Compared with FI action on metallic tips, requiring 100 times stronger fields ( $10^8$  V cm $^{-1}$ ), and producing currents of the order of pico- to microamperes, it is clear that both the required field and the measured currents turned out to be dramatically lower here. As a result, the first assumption of FI occurring at a smaller critical distances on semiconductors is ruled out. This is in contrast with the earlier work, where enhanced FI was explained on the basis of  $d_{c\text{-semicond}}$  being less than  $d_{c\text{-metal}}$  (ref. 15). Table 1 summarizes the results of some earlier field-ion  $I$ - $V$  measurements, mainly during field-ion microscopy. Data were extracted from the  $I$ - $V$  curves in the field-limited regime. The last row contains the result of this work, showing a reduction of about two orders of magnitude in the field. Note that the sub-10 V helium FI of Singh *et al.* on  $\beta$ -W nanorods was due to the large field enhancement of atomically sharp nanorod tip apices, in the range of 0.1–0.2 nm, capable of generating 0.5–1.0 V Å $^{-1}$  (ref. 16).

**Table 1 | FI on different tip materials compared with our whiskered silicon nanowires.**

Tip material	$r_t$ (nm)	Tip voltage	Field strength* ( $\times 10^8$ V cm $^{-1}$ )	Current (A)	Gas	Pressure (torr)	Reference
Ir	100	12 kV	2.4	$4.0 \times 10^{-10}$	H <sub>2</sub>	$10^{-3}$	Fig. 4 of ref. 7
Ir	80–150	15 kV	2.4	$10^{-10}$	H <sub>2</sub>	$10^{-2}$	Fig. 5 of ref. 20
Ge	250	17.8 kV	1.4	$6.3 \times 10^{-14}$	Ar	$2 \times 10^{-6}$	Fig. 3 of ref. 21
W	100	-	1.3	$10^{-10}$	Ar	$\sim 10^{-6}$	Fig. 3 of ref. 22
W	Single atom	1.6 kV	-	-	Ar	$8.4 \times 10^{-6}$	Ref. 23
$\beta$ -W	0.1–0.2	3–4 V	0.5–1.0	$\sim 10^{-10}$	He	$10^{-5}$ – $10^{-2}$	Ref. 16
Si/Au nanowhiskers	$\sim 10$	6 V	0.018 (maximum)	$7 \times 10^{-22}$	N <sub>2</sub>	$2.5 \times 10^{-6}$	This work

\*Values of the field magnitude are shown here if available in the references, or the maximum value was suggested on the basis of  $F_{\max} = V/5r_t$ .

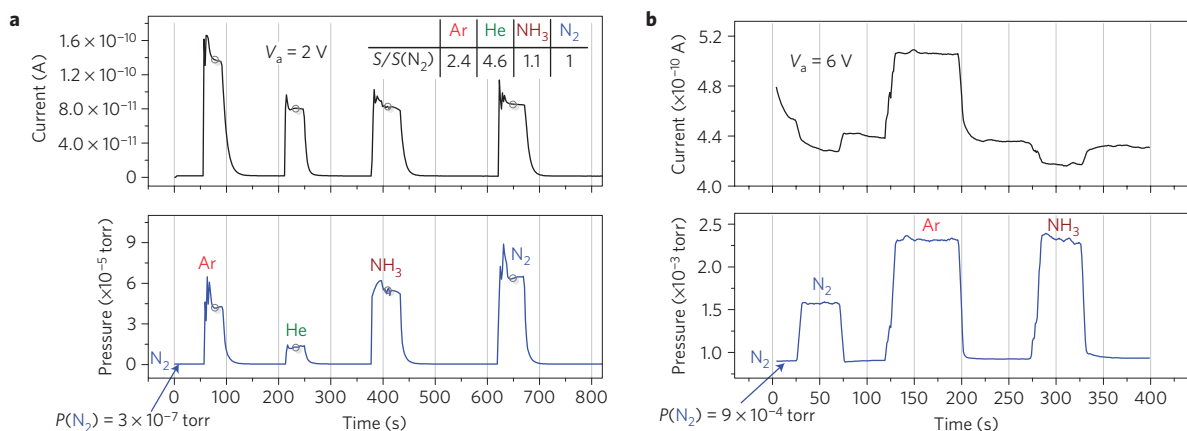


**Figure 5 | Sensitivity and the effect of gas admixtures on the low-voltage field-ion current.** **a**, Continuous ionization current of argon, helium, ammonia and nitrogen, on undoped whiskered nanowires at a bias of  $V = 2$  V. Points from which the sensitivities,  $S = I/V$ , were taken are indicated by circles. Values of  $S$  are normalized to that of nitrogen and shown in the table in the inset. **b**, The ionization discharge current on whiskered silicon nanowires is measured at a bias of  $V = 6$  V. The background gas is nitrogen at  $9 \times 10^{-4}$  torr, while nitrogen, argon and ammonia were injected sequentially. The lower panel shows the total pressure. The current increases in the presence of argon, but it decreases for the other two gases because of a greater  $S$ .

We suggest two other possible mechanisms capable of describing the above phenomena. As Ohno *et al.* have suggested, the shape of the potential barrier changes from triangle to trapezoid with the increase of the surface work function and the decrease of the image field as illustrated in Fig. 4b (ref. 14). This model presumes that the tunnelling distance is almost equal in both cases, whereas the lower current is due to a larger and wider potential barrier. In other words, field penetration affects not  $d_c$  but the imaging field. As a result, the field-ion current on semiconductors was shown to be about  $10^4$  times smaller than on metals (note for example Ge versus Ir in Table 1). The effect of surface states was not considered in this model. Nevertheless, as shown in Fig. 4c, tunnelling may occur into these states even without surface inversion. The presence of surface states associated with impurities affects the band bending potential as well, even in a field-free case. Under an applied field, charging of these states can reduce the amount of band bending<sup>6</sup> (surface-state shielding). Recently, Garnett *et al.* have measured the interface-state density of a 75 nm VLS-grown silicon nanowire to range from  $4 \times 10^{11}$  cm $^{-2}$  eV $^{-1}$  at mid-gap to  $10^{13}$  cm $^{-2}$  eV $^{-1}$  close to the valence-band edge<sup>17</sup>. Within this range, surface-state shielding seems to be negligible in VLS-grown nanowires. In addition, the higher number of edge sites is in favour of tunnelling from farther molecules (larger  $d_{c-\text{semicond}}$ ) and at lower fields (see Fig. 4c).

Our observations on the inception of FI action at sub-10 V voltages are more consistent with the surface-state model. In general, tunnelling into the states close to the valence band is easier because of the shorter  $d_c$  the ionizing particle will encounter<sup>18</sup>.

As no FI current was detected on the whiskered nanowire sample after catalyst removal, we deduce that the surface states are indeed sourced from gold. The ratio of ion currents emitted from each silicon nanowhisker to the nominal currents obtained on metallic tips is about  $10^{-11}$  (for example, from Table 1,  $I_{\text{SiNW}}/I_W = 7 \times 10^{-22}/10^{-10} \approx 10^{-11}$ ). Equation (3) gives a  $d_c$  of roughly a few more ångströms for FI on silicon whiskers, assuming  $\Delta V$  not to vary significantly in the two cases. Even if  $\Delta V$  is to be considered, such low currents agree well with the fact that tunnelling occurs from distant particles as illustrated in the energy band diagram of Fig. 4c.

### Sensitivity

To examine the relative sensitivity of the field ionizer to various gases, test gases were sequentially injected into the vacuum chamber, while the device was biased at 2 V. Figure 5a shows the resultant currents. We define the ratio of the current corresponding to each gas to its partial pressure,  $S = I/P$ , as a measure of sensitivity. The table in the inset shows the values of  $S$  normalized to that of nitrogen. We also studied the low-field FI behaviour in gas admixtures by carrying out temporal injection of nitrogen, argon and ammonia, respectively, in a nitrogen atmosphere ( $P \sim 9 \times 10^{-3}$  torr). This pressure-bias point lies within the range where current slightly decreases with pressure. Figure 5b shows the resulting anode current versus time. On the basis of the curve in the inset of Fig. 3a, the current drop for the cases of nitrogen and ammonia is predictable. However, injection of argon has caused a significant increase in the total current, even though the ionization potentials of nitrogen and argon

are very close, and the polarizabilities are not very different either ( $U_1(\text{N}_2) = 15.6 \text{ eV}$ ,  $U_1(\text{Ar}) = 15.75 \text{ eV}$ ,  $\alpha(\text{N}_2) = 1.74 \text{ \AA}^3$  and  $\alpha(\text{Ar}) = 1.64 \text{ \AA}^3$ ; ref. 19). We believe this is due to the higher sensitivity of the device to argon than to nitrogen, as it can be clearly seen in Fig. 5a that argon has produced a higher current than nitrogen at comparable partial pressures. A similar effect was observed when argon was used as the host gas (see Supplementary Information).

## Conclusion

We have demonstrated occurrence of anomalously strong FI on gold-catalysed whiskered silicon nanowires and explained our observations on the basis of combination effects of geometrical field enhancement and silicon surface states close to the gold–silicon interface at the whisker tips. Although unintentional incorporation of impurities in nanowires from the catalysts adversely affects the electrical properties and impedes the development of high-performance electronic and photonic devices, the application of nanowires grown by VLS processes offers a unique advantage for FI applications by offering nanostructures with unmatched dimensions that readily come with high density of surface states associated with the impurities and dangling bonds. To precisely quantify and predict the magnitude of semiconductor-assisted field-ionization, field-desorption and field-evaporation processes, systematic measurements are required to find the position and density of gold-induced surface states. In addition, because the anomalous enhancement of field-ion currents measured in this work was correlated with geometrical amplification of the field on whisker tips, it was difficult to quantify these two effects separately. Future work can focus on engineering confined surface levels with known density and location at sharp semiconductor surfaces. In this case, low-voltage FI can offer implications for accurate fingerprinting of gases, for instance in bio-chemical, environmental and disease-sensing applications.

## Methods

**Synthesis of smooth and whiskered Si nanowires.** Whiskered silicon nanowires were synthesized by a two-step VLS technique using  $\text{SiH}_4$  as the precursor. A 3-nm-thick layer of Au was first evaporated on ultraclean oxide-free p-type Si(111) substrates, with a volume resistivity of  $\rho < 0.005 \text{ } \Omega \text{ cm}$ . The substrates were then heated at  $610 \text{ }^\circ\text{C}$  for 20 min in 10 torr  $\text{H}_2$  to form Au–Si alloy and then dewet the film, creating alloy droplets. Primary nanowires (nanowire trunks) were grown at  $680 \text{ }^\circ\text{C}$ , for 1 h under 15 s.c.c.m. flow of  $\text{SiH}_4$ . Next, the samples were annealed for 5 min by introducing 15 s.c.c.m. HCl into the chamber, while the temperature was ramped down from 680 to  $580 \text{ }^\circ\text{C}$ . HCl was used to inhibit upward growth of primary nanowires and cause downstream migration of the Au–Si eutectic.  $\text{SiH}_4$  was then reintroduced into the chamber at the same rate for 5 min to form the whiskers from the alloy that was spread during the intermediate annealing step. For smooth nanowires, the last step was not carried out. Whiskered nanowires were boron doped by flowing 3.0 s.c.c.m.  $\text{B}_2\text{H}_6$  (100 ppm in  $\text{H}_2$ ) during the growth. Gold nanoparticles were removed from the tips by immersion into a solution consisting of 9:1 (parts by volume) commercial triiodide etchant (Transene):36% HCl, for 20 s.

**Current–voltage–pressure measurements.** Cylindrical ionization cells were fabricated on both smooth and whiskered Si nanowires. A secondary circular flat electrode (aluminium) was mounted on the samples using a 100- $\mu\text{m}$ -thick polypropylene film. The film contained patterned channels to facilitate flow of gas (see Fig. 2e). Ohmic connections were made to both electrodes. The devices were installed in a custom-made vacuum chamber with electrical feedthroughs and mass flow controllers capable of regulating the output flow rate down to 1 s.c.c.m. Frequent purging with dry nitrogen ensured total removal of water vapour. The pressure was kept precisely constant by a proportional–integral–derivative controller during the course of each voltage sweep. Two source measure units connected separately to each electrode were used to carry out a staircase sweep, one in the positive direction and the other in the negative direction. To ensure that the charging current due to the cell capacitance was negligible, the sweep parameters were chosen as  $\Delta V < 1 \text{ V}$  and  $\Delta t = 50 \text{ ms}$ .

Received 4 December 2009; accepted 14 December 2010; published online 16 January 2011; corrected online 1 February 2011

## References

- Li, F., Xie, Z., Schmidt, H., Sielemann, S. & Baumbach, J. I. Ion mobility spectrometer for online monitoring of trace compounds. *Spectrochim. Acta B* **57**, 1563–1574 (2002).
- Riley, D. J. *et al.* Helium detection via field ionization from carbon nanotubes. *Nano Lett.* **3**, 1455–1458 (2003).
- Modi, A., Koratkar, N., Lass, E., Wei, B. & Ajayan, P. M. Miniaturized gas ionization sensors using carbon nanotubes. *Nature* **424**, 171–174 (2003).
- Velasquez-Garcia, L. F. & Akinwande, A. I. *Micro Electro Mechanical Systems*. IEEE 21st International Conference on, 2008, 742–745 (2008).
- Gomer, R. *Field Emission and Field Ionization* (Harvard Univ. Press, 1961).
- Miller, M. K., Cerezo, A., Hetherington, M. G. & Smith, G. D. W. *Atom Probe Field Ion Microscopy* (Oxford University Press, 1996).
- Liu, X. & Orloff, J. Analytical model of a gas phase field ionization source. *J. Vac. Sci. Technol. B* **23**, 2816–2820 (2005).
- Doerk, G. S., Ferralis, N., Carraro, C. & Maboudian, R. Growth of branching Si nanowires seeded by Au–Si surface migration. *J. Mater. Chem.* **18**, 5376–5381 (2008).
- Müller, E. W. & Tsong, T. T. *Field Ion Microscopy; Principles and Applications* (American Elsevier Pub., 1969).
- Forbes, R. G., Edgcombe, C. J. & Valdre, U. Some comments on models for field enhancement. *Ultramicroscopy* **95**, 57–65 (2003).
- Read, F. H. & Bowring, N. J. Field enhancement factors of random arrays of carbon nanotubes. *Nucl. Instrum. Methods Phys. Res.* **519**, 305–314 (2004).
- Banan-Sadeghian, R. & Kahrizi, M. *COMSOL Multiphysics Conf.* 251–254 (2005).
- Willardson, R. K. & Beer, A. C. *Semiconductors and Semimetals: Injection Phenomena* (Academic, 1970).
- Ohno, Y., Nakamura, S. & Kuroda, T. Mechanisms of field ionization and field evaporation on semiconductor surfaces. *Jpn. J. Appl. Phys.* **17**, 2013–2022 (1978).
- Banan-Sadeghian, R. & Kahrizi, M. A novel gas sensor based on tunneling-field-ionization on whisker-covered gold nanowires. *IEEE Sensors J.* **8**, 161–169 (2008).
- Singh, J. P., Karabacak, T., Lu, T. M., Wang, G. C. & Koratkar, N. Field ionization of argon using  $\beta$ -phase W nanorods. *Appl. Phys. Lett.* **85**, 3226–3228 (2004).
- Garnett, E. C. *et al.* Dopant profiling and surface analysis of silicon nanowires using capacitance–voltage measurements. *Nature Nanotech.* **4**, 311–314 (2009).
- Ohno, Y., Nakamura, S., Adachi, T. & Kuroda, T. Field-ion microscopy of GaAs and GaP. *Surf. Sci.* **69**, 521–532 (1977).
- Gao, K., Yan, M., Feng, M. & Zhu, X. Measurement of charge-transfer rate coefficients between  $\text{Co}^{3+}$  and Ar,  $\text{N}_2$  at electron-volt energy. *J. Phys. B* **35**, 233–240 (2002).
- Orloff, J. H. & Swanson, L. W. Study of a field-ionization source for microprobe applications. *J. Vac. Sci. Technol.* **12**, 1209–1213 (1975).
- Ernst, L. & Block, J. H. Field ion microscopy of germanium: Field ionization and surface states. *Surf. Sci.* **49**, 293–309 (1975).
- Müller, E. W. & Bahadur, K. Field ionization of gases at a metal surface and the resolution of the field ion microscope. *Phys. Rev.* **102**, 624–634 (1956).
- Moh'd, R., Jason, P. & Robert, W. Tungsten nanotip fabrication by spatially controlled field-assisted reaction with nitrogen. *J. Chem. Phys.* **124**, 204716 (2006).

## Acknowledgements

The work reported herein was partially supported by the Natural Sciences and Engineering Research Council (NSERC) of Canada, a University of California CITRIS research grant funded by Hewlett Packard Labs, NSF grant 0547679 and an Army Research Office (ARO) research grant 55176-EL-DRP. R.B.S. would like to thank J. Y. Oh for help with nanowire synthesis, Logeeswaran VJ for help with the vacuum chamber set-up and A. Ghogha for help with statistical analysis.

## Author contributions

R.B.S. designed and carried out experiments, analysed data and wrote the manuscript. M.S.I. supervised the project, analysed data and edited the manuscript. Both authors discussed the results, and commented on the manuscript.

## Additional information

The authors declare no competing financial interests. Supplementary information accompanies this paper on [www.nature.com/naturematerials](http://www.nature.com/naturematerials). Reprints and permissions information is available online at <http://npg.nature.com/reprintsandpermissions>. Correspondence and requests for materials should be addressed to M.S.I.

# ULTRALOW-VOLTAGE FIELD-IONIZATION DISCHARGE ON WHISKERED SILICON NANOWIRES FOR GAS-SENSING APPLICATIONS

Supplementary Information

by: Ramin Banan Sadeghian and M. Saif Islam

**1) Analysis on the dimension of whiskers and field enhancement:** The total number of silicon nanowhiskers ( $N_{\text{whsk}}$ ) was roughly estimated by multiplying the number of whiskers counted on a single primary nanowire by the number of primary nanowires at the anode. The following illustrations demonstrate the details of our analysis in sequence (abc).

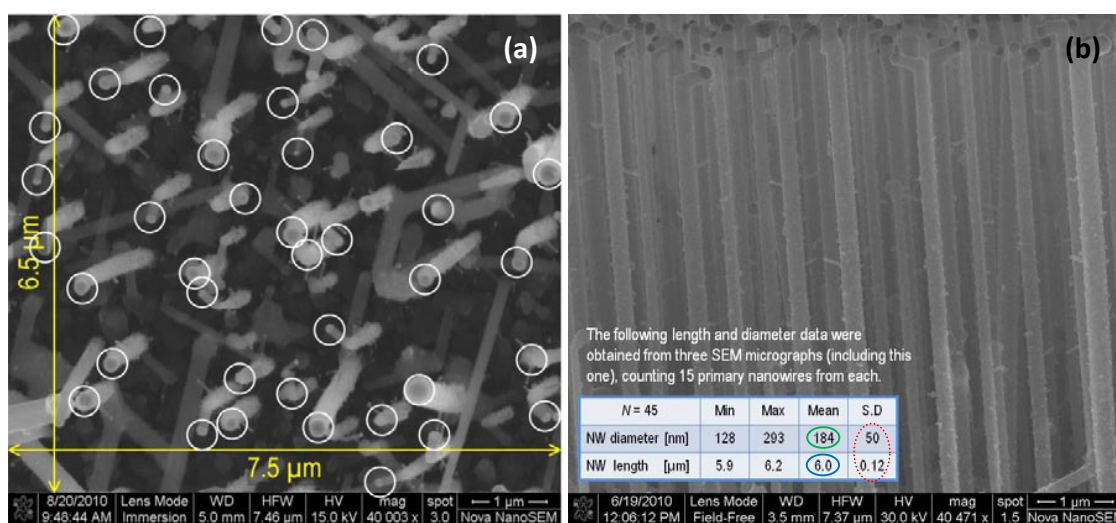
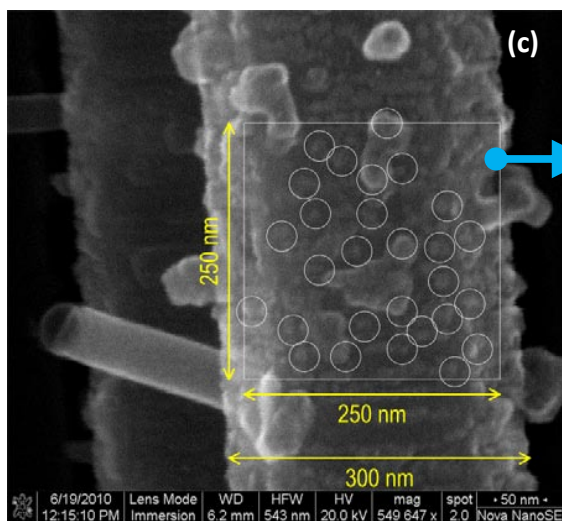


**Fig. 1. (a)** Density of primary Si nanowires was estimated by counting the nanowire tips.

**(b)** Length and diameter data were obtained from cross sectional SEM images.



**(c)** The total density of whiskers (clearly discernable protrusions along with tiny nanoscale buds) was obtained by counting them in measured areas of primary nanowires.

- Density of primary nanowires =  $8.4 \times 10^{11} \text{ m}^{-2}$ .
  - Total no. of primary nanowires = Au-coated area  $\times 8.4 \times 10^{11} \text{ m}^{-2} = 9.2 \times 10^7$ .
  - Projected area =  $9.4 \times 10^{-14} \text{ m}^2$ .
  - Average NW area =  $A_{NW} = \pi 2\bar{r}\bar{l} = 3.5 \times 10^{-12} \text{ m}^2$ , where  $2\bar{r}$  and  $\bar{l}$  are the mean diameter and length of nanowire trunks obtained at step (b).
  - Whiskers per nanowire = 1279.
  - Total number of whiskers =  $1279 \times 9.2 \times 10^7 = 1.2 \times 10^{11} \approx 10^{11}$ .
- Only the uncertainty in primary nanowire diameters and lengths were accounted for in this estimation. All other numbers such as the whisker density are average values.

Figures 2a-c show histograms of the whisker dimensions extracted from SEM micrographs. The prominent whiskers refer to those which have fully protruded out of the primary nanowire. The

diameter distribution of all of the whiskers is presented separately. Here we show that even if the maximum field enhancement is achieved at the apex of the whiskers, the local field therein is far less than  $V/\text{\AA}$ , usually required for field ionization. Because of the relatively large distribution of the size of the whiskers it is impractical to obtain a single field-enhancement factor for the system, thus the maximum is considered.

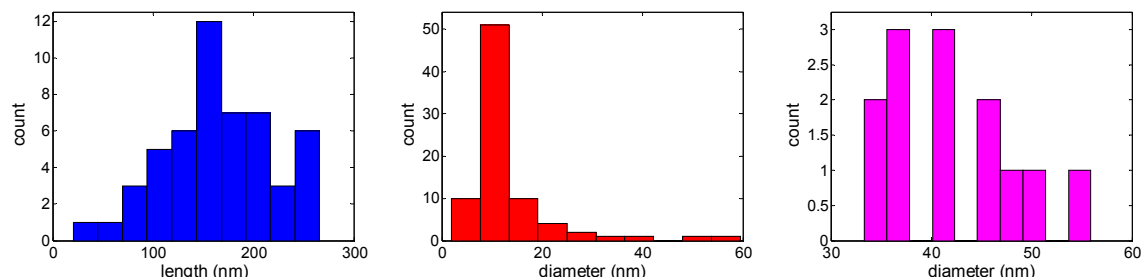


**Fig. 2a)** Length of the prominent whiskers with a mean at  $l = 165$  nm.

**b)** Diameter of all of the whiskers, including the tiny ones encircled in **Fig. 1c**. The mean is at  $2r = 13.3$  nm.

**c)** Diameter of the prominent whiskers, discernible in **Fig. 1b**. The mean is at  $2r = 42.3$  nm.

According to the field enhancement model of a hemisphere on post structure, which can be perfectly applied to the prominent whiskers [1], the estimated field enhancement factor is given by

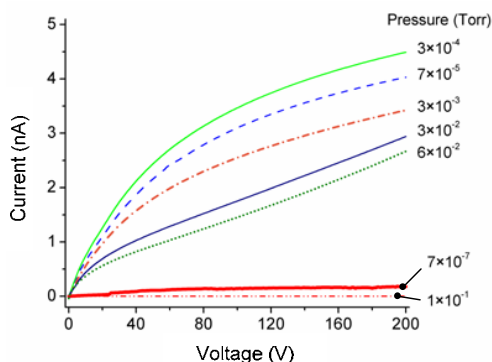
$$\gamma_a = 1.2(2.15 + \nu)^{0.9}, \quad (1)$$

where  $\nu = \bar{l}/\bar{r} = 165/21.1 = 7.8$  is the ratio of protrusion length to base radius. Note that the above model is valid when the scale of the protrusion is much smaller than the interelectrode separation ( $100\mu\text{m}$ ). In addition, because the protrusions are much larger than atomic scale, there is no quantum confinement to affect the distribution of electron charge and the field distribution deduced from the atomic-level charge distribution on the tips, so  $\gamma_a$  is not affected by this matter [2-3]. Equation (1) gives a value of  $\gamma_a = 9.5$  which corresponds to a local field (at the apex of whisker) of  $9.5 \times 10^3$  V/cm at an applied field of  $10\text{V}/100\mu\text{m} = 10^3$  V/cm ( $100\mu\text{m}$  is the electrode spacing). Therefore, the probability of *classic* tunneling field ionization (i.e. tunneling into metallic tips) which require field strengths in the order of  $V/\text{\AA}$ , ( $10^8$  V/cm) is absolutely slim. To emphasize the fact that even the highest possible field enhancement factor obtainable at the sharpest feature in our many-nanowire system is not sufficient to generate field strengths in the order of  $V/\text{\AA}$ , in the manuscript we have considered the upper limit of the local field achievable at the apex of the smallest protrusion, a whisker with a diameter of  $2r = 13.3$  nm. The maximum local field at a sharp tip is given by  $F_{loc} = V/5\bar{r}$  ( $V/r$  for a floating sphere) [4], resulting a local field of  $F_{loc} = 3.0 \times 10^6$  V/cm, or an enhancement factor of  $\gamma_a = F_{loc}/F_{applied} = (V/5r)/(V/d) = d/5r = 100\mu\text{m}/(5 \times 0.0067\mu\text{m}) \approx 3000$ , which is still too small to generate measurable field ionization if classic tunneling field ionization is accounted for.

It is imperative to note that, in contrast to previous works such as that of [5], where the applied and local fields were very large because of the small gap spacing ( $d \approx 1.1\mu\text{m}$ ) and atomically sharp tips respectively, FI on our silicon whiskers happens at much lower fields, within a larger gap ( $d = 100\mu\text{m}$ ). A larger gap can accommodate a higher gas volume and is especially favorable for a gas ionization sensing.

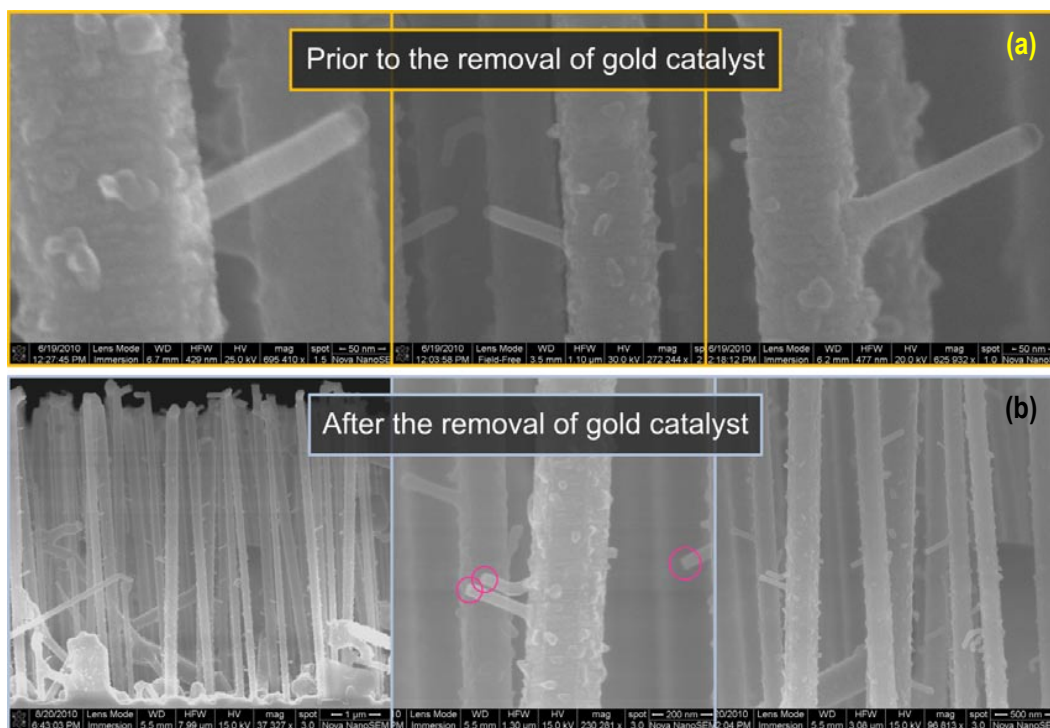
**2) Current-Voltage characteristics of smooth silicon nanowires:** To further support the argument that low-voltage FI phenomenon originates from the whiskers, we run the experiments on whiskerless nanowires. Smooth nanowires were grown by the same VLS process used to grow whiskered types, without reintroducing the Si precursor gas ( $\text{SiH}_4$ ) after the annealing step. As a result, nucleation and

growth of whiskers after downward migration of Au-Si eutectic did not occur. No trace of anomalous FI action was detected on these whiskerless nanowires and the discharge characteristics followed that of geometries resembling parallel-plate configurations. As shown in Fig. 3, the discharge currents begin in the ohmic regime and then tend to saturate. The density of electron current to the anode is given by  $J_a = e \cdot d \cdot (dn/dt)$ , where  $d$  is the gap spacing, and  $(dn/dt)$  is the total rate of carrier generation per unit volume.  $J_a$  is expected to be invariant with respect to voltage before the Townsend electron multiplication mechanism takes effect [6].



**Fig. 3.**  $I$ - $V$  curves recorded in different pressures of nitrogen using whiskerless nanowires.

**3) Disappearance of anomalous FI action after removal of gold tips:** We employed McIntyre's method [7] to remove the gold from the nanowhisker tips using aqueous triiodide and HCl. The SEM micrographs presented below show that the etchant has completely removed gold nanoparticles without disturbing the nanowire network and the geometry of whiskers. Similar to the case of smooth nanowires, no enhanced ionization currents were probed using the gold-less samples within the voltage range studied. Figure 4c shows the  $I$ - $V$  obtained from the sample after gold removal.



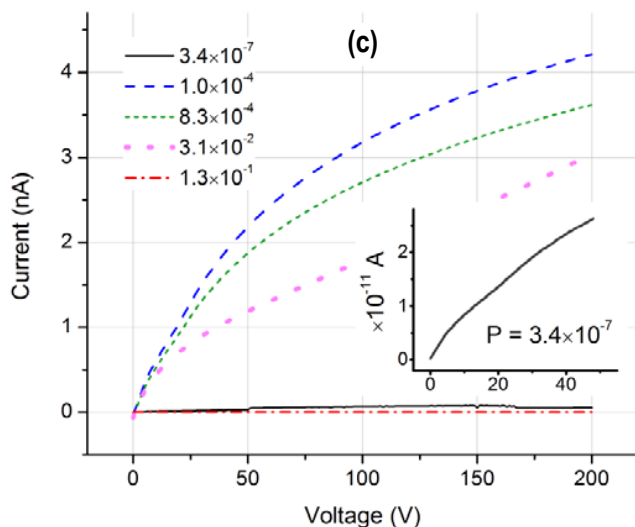


**Fig. 4. Top (a,b):** It is clear that after the etching treatment, the body of the silicon whiskers as well as the tiny nanoscale buds have remained untouched. We can conclude that the tiny protrusions, even some of which too small to be seen in the SEM images are made of *silicon* and contribute to metal catalysed semiconductor-assisted field ionization with their catalyst intact.

**Left (c):** *I-V* curves obtained from whiskered nanowires after the removal of gold catalyst. Note the resemblance between these curves and those obtained from **whiskerless** Si nanowires. Measurements were carried out in different gas ( $N_2$ ) pressures. The magnified *I-V* curve at the inset corresponds to  $P = 3.4 \times 10^{-7}$  Torr.

**4) Effect of p-type doping:** we conducted p-type doping of the nanowires using diborane ( $B_2H_6$ ) (100 ppm in  $H_2$ ) as the dopant source during the growth of the whiskers. As shown in the table below, only whiskers doped with a  $B_2H_6$  flow rate of 3 sccm (Sample #2) displayed improvement of the field-ion currents over our initial measurements on undoped samples (e.g. Sample #1). Whiskers doped with higher diborane flow rates did not exhibit the anomalous effect at all. Diborane ( $B_2H_6$ ) decomposes to form monoborane ( $BH_3$ ) which reacts with silane ( $SiH_4$ ) leading to an enhancement in the amorphous silicon thin film deposition rate [8]. When  $B_2H_6$  flow rate is considerably increased, the increased silicon thin film deposition rate results in the formation of an amorphous silicon layer on the outer surface of the nanoscale whiskers. Earlier reports [8-9] suggest that high flow rate of diborane can cause considerable amorphization of the nanowire surface whose effect on FI is not understood. In this work, although we did not observe a discernable change in the morphology of SiNWs as reported in [9], we believe high flow rate of  $B_2H_6$  (above 3 sccm) has contributed to a change in the physical properties of the whiskers resulting in a sudden cut-off in FI property.

**Table I.** VLS growth parameters

Sample #	Annealing		Primary growth		Secondary growth		Silane flow rate (sccm)	$B_2H_6$ flow rate (sccm)	Enhanced ionization
	Temp (°C)	Time (min)	Temp (°C)	Time (min)	Temp (°C)	Time (min)			
1	610	20	680	60	580	5	15	–	✓
2	610	20	680	60	580	5	15	<b>3</b>	✓
3	610	20	680	60	580	5	15	<b>5</b>	✗
4	610	20	680	60	580	5	15	<b>30</b>	✗
rest	Sampled with different annealing/growth/flow rate conditions did not show the anomalous ionization effect.								✗

At lower voltages, where we believe field ionization instigates, the amplitudes of the probed currents do not vary considerably between the devices made of unintentionally doped and moderately doped samples. This suggests that the field ionization current may not be a strong function of the the Fermi level position in the bulk of protrusions. Perhaps tunneling into the empty states of the degenerate surface is scarce (see **Figure 4c** of the manuscript), as compared to the rate of tunneling into the surface states. **Figure 4c** emphasizes on the hypothesis that tunneling can be more desirable into surface states that into the empty surface states above  $E_F$ . However, the doped sample has exhibited larger currents at higher voltages where the current is limited by the resistance of the protrusions. Diborane doping did not affect morphology of the nanowire network.

**5) Estimation of the increase in the tunneling distance ( $d_c$ ) on our Si whiskers as compared to metallic specimens:** Using WKB approximation, Gomer [3] has calculated the triangular barrier penetration probability as:

$$D = \exp\left\{-0.683(I - 7.59F^{1/2})^{1/2} \frac{(I-\phi)}{F}\right\}, \quad (2)$$

where  $F$  is the field strength in  $V/\text{\AA}$ ,  $I$  is the ionization potential ( $U_i$ ) in eV, and the barrier base (critical distance) is  $d_c = \frac{(I-\phi)}{eF}$  in  $\text{\AA}$ . Using the coefficients of the Gomer's equation and the methodology introduced in equation (4) of the manuscript, for nitrogen with a Best-Image-Field (BIF) of  $F_{\text{metal}} = 1.7 \text{ V/\AA}$  on metal tip, and assuming  $d_{c\text{-metal}} \approx 4 \text{ \AA}$ , and  $F_{\text{semicond}} \ll F_{\text{metal}}$ , a tunneling distance of  $d_{c\text{-semicond}} \approx 13.7 \text{ \AA}$  (i.e.  $\Delta d_c = 9.7 \text{ \AA}$  longer than on a metal tip) is calculated. A similar result is obtained, using Ohno and coworkers' formalism (see equation (6) of [10] with  $x_0 = 0 \text{ \AA}$ ).

**6) Field Ionization in a background atmosphere:** In addition to  $N_2$  as explained in the manuscript, we used Ar as a background gas and measured modulation of the steady ionization currents by introducing guest gases:  $N_2$ , Ar, He and  $NH_3$ . In an  $N_2$  background and for either samples, the current increased by injecting Ar and other gases.

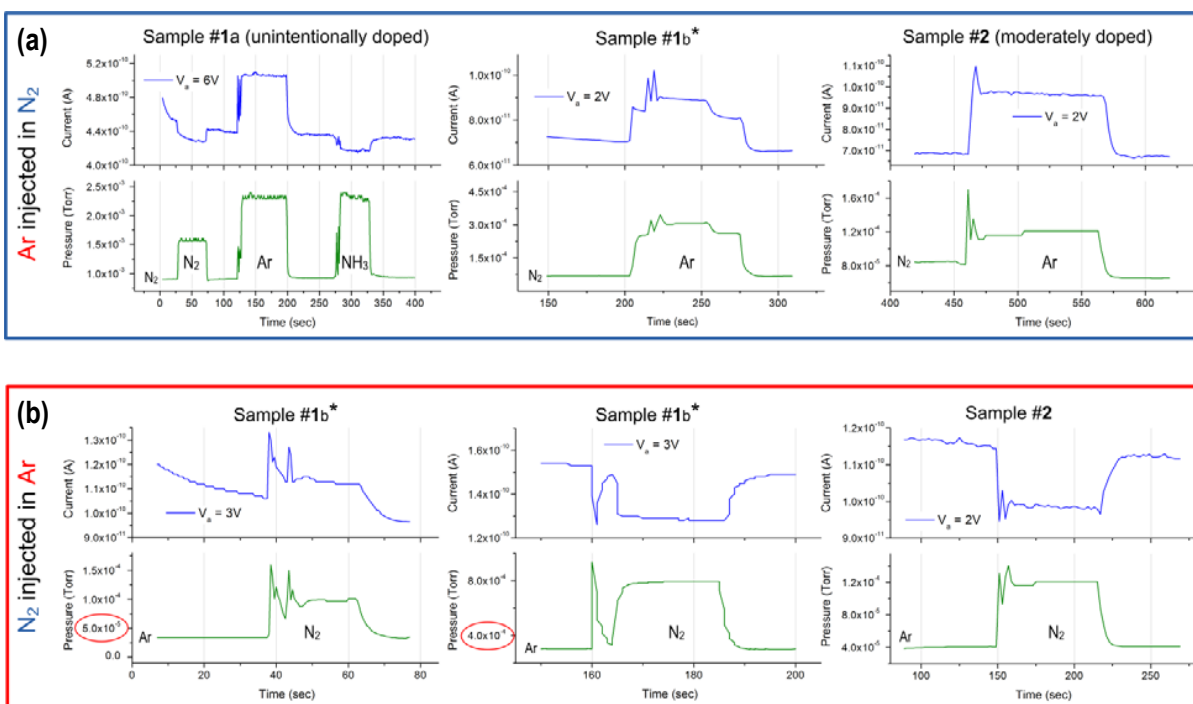


**Fig. 5.** Mutual effects of Ar and  $N_2$  on the ionization currents; **Top:** Irrelevant to the doping level of samples, injection of Ar gas into  $N_2$  background boosts the ionization currents at a steady bias voltage. **Bottom:** While  $N_2$  injected in Ar has had a similar effect on Sample #1, the reverse effect was observed in Sample #2 (doped) and Sample #1 in a higher background pressure.

\* Sample #1a and Sample #1b refer to two different samples grown using same growth parameters (same VLS growth recipe).

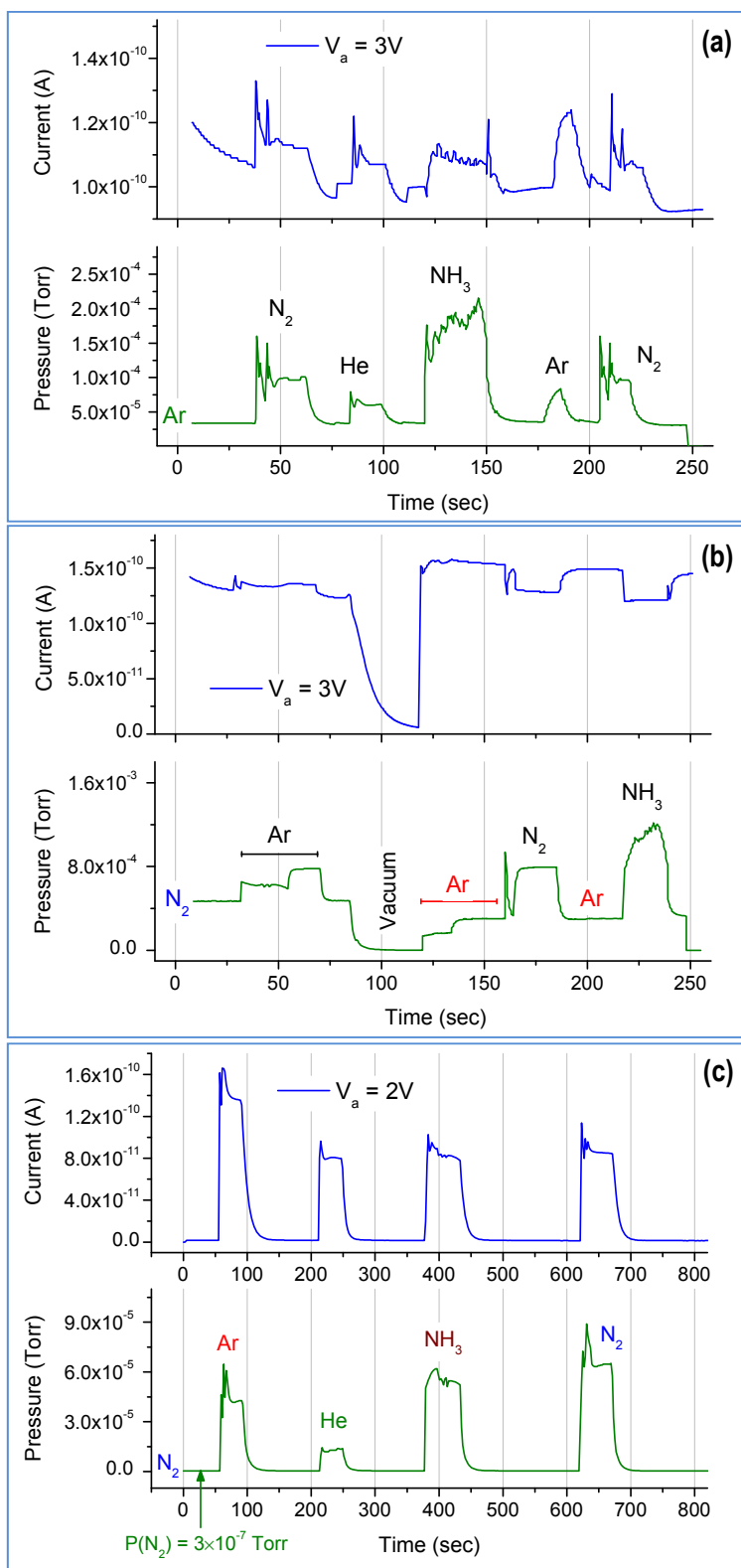


**Fig. 6.** Effect of various foreign gases on the enhanced ionization currents of argon and nitrogen as host gases. Data are extracted from Sample #1b.

During steady state operation, that is when the bias is fixed, we define the ratio of the modulated current corresponding to each gas to its partial pressure,  $S = I_a/P$ , as a measure of sensitivity. The following table shows the values obtained from the above curve (c). The reason that the field ionization current of Ar gas drops when  $N_2$  is injected at higher partial pressures of  $N_2$ , can be because of a less sensitivity of Sample #1b and Sample#2 to  $N_2$  than to Ar. As a result, when the admixture contains more nitrogen than argon, the overall current drops.

**Table II.** Sensitivity of Sample #1b to various gases at  $V_a = 2$  V.

Injected gas	Ar	He	$NH_3$	$N_2$
Sensitivity (A/Torr)	$3.28 \times 10^{-6}$	$6.26 \times 10^{-6}$	$1.51 \times 10^{-6}$	$1.36 \times 10^{-6}$

7) In order to examine the stability of the currents observed in this work, we measured the changes in the sensitivity ( $S$ , as defined above) of Sample #1a after successive voltage sweeps. The curves showing evolution of  $S$  through five sequential runs (voltage sweeps of 0 to 100 V) are plotted in Fig. 7.  $S$  was measured during the sweep at two different biases: **(a)**:  $V_a = 10$  V, **(b)**:  $V_a = 20$  V. It is clear that the FI strength deteriorates with time.

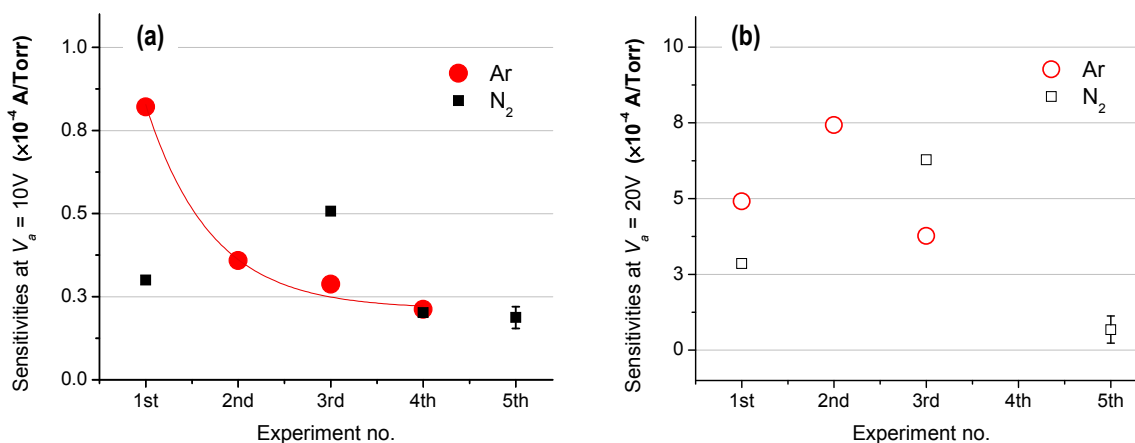


**Fig. 7.** Discernable decrease in the sensitivity of Sample #1a to argon and nitrogen, after five voltage sweeps, measured at **a)**  $V_a = 10$  V and **b)**  $V_a = 20$  V.

By comparing the SEM images taken from a fresh sample and those taken after the whiskers have undergone field ionization under the highest applied bias voltage (200 V), we observed that the macro morphology of the whiskers is not affected. Nevertheless, the enhanced current abruptly ceased at this voltage and afterwards the device behaved like its whiskerless nanowire counterpart. It is not clear yet why degradation of wires is not observed in the SEMs while there is a discernable loss of FI property.

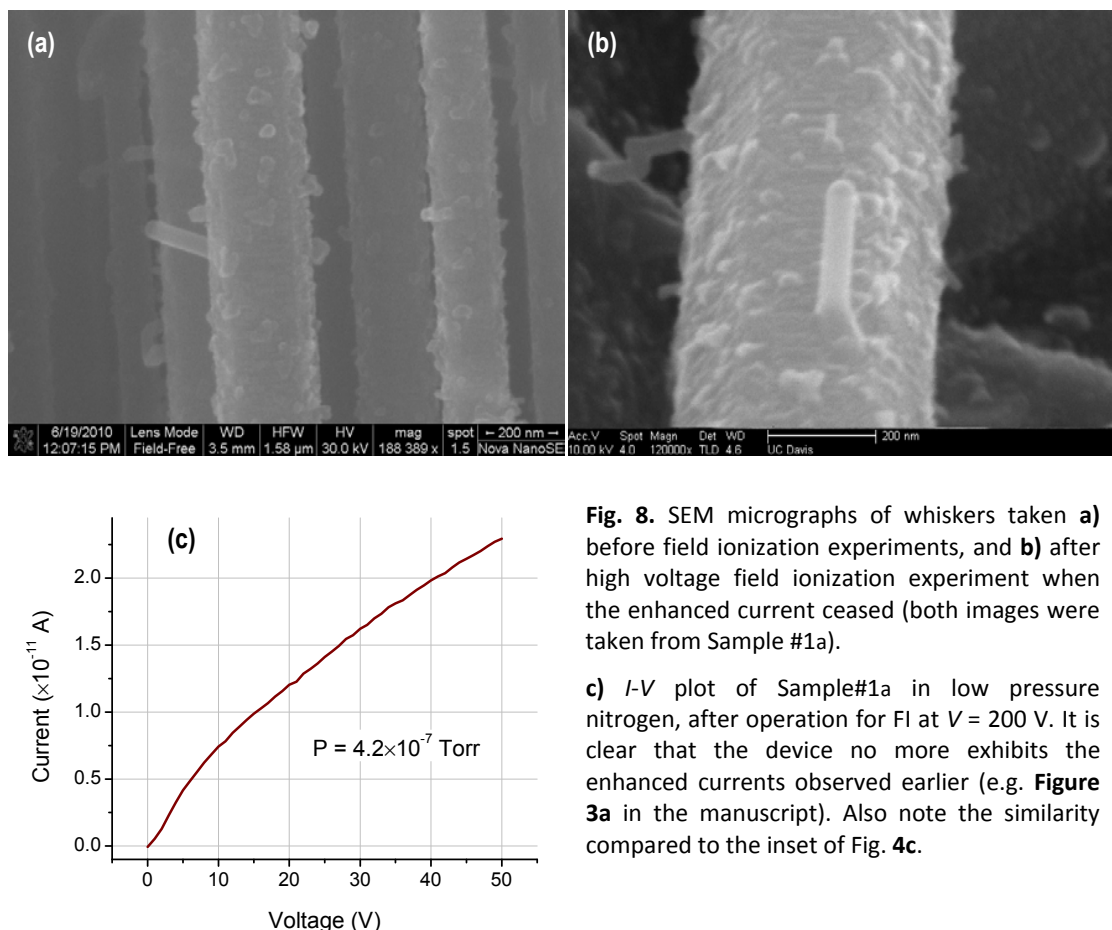


**Fig. 8.** SEM micrographs of whiskers taken **a)** before field ionization experiments, and **b)** after high voltage field ionization experiment when the enhanced current ceased (both images were taken from Sample #1a).

**c)** *I-V* plot of Sample#1a in low pressure nitrogen, after operation for FI at  $V = 200$  V. It is clear that the device no more exhibits the enhanced currents observed earlier (e.g. **Figure 3a** in the manuscript). Also note the similarity compared to the inset of **Fig. 4c**.

**8) On the variety and effectiveness of surface states:** Ernst has argued that if the surface state density is less than  $10^{13} \text{ cm}^{-2} \text{ eV}^{-1}$ , the surface state shielding of band bending can be neglected in the relevant energy region so the applied field will be entirely consumed by band bending [11]. Assuming field penetration and band bending in the near surface layers of our silicon nanowires not to differ appreciably from those of a planar substrate [12], we can state that surface state shielding would be negligible in our case too. According to Seo et al, and Kimukin et al, the surface density for VLS grown silicon nanowires, covered with native oxide, is in the order of  $2 \times 10^{12} \text{ cm}^{-2}$  [13-14] which is readily less than the limit calculated by Ernst, even if the entire band gap is filled with surface states. Also recently, Garnett et al. have measured the interface state density of a 75 nm VLS-grown silicon nanowire to range from  $4 \times 10^{11} \text{ cm}^{-2} \text{ eV}^{-1}$  at mid-gap to  $10^{13} \text{ cm}^{-2} \text{ eV}^{-1}$  close to the valance band edge [15], which is also less than Ernst's limit for surface state shielding. Interestingly, the higher number of edge sites is in favor of tunneling from farther molecules (larger  $d_{c\text{-semicond}}$ ) and at lower fields (see **Figure 4c** in the manuscript).

Earlier reports on the existence of wide band surface states close to the valance band, include Eastman and Grobman's 0.8–1.0 eV wide band, centered at 0.45 eV below  $E_V$  on a lightly doped *n*-type sample [16], and Wagner and Spicer's, 1.8 eV wide band, with a density of  $8 \times 10^{14} \text{ cm}^{-2}$  on a highly doped *n*-type Si (111) sample [17]. In addition to the surface states due to dangling bonds and defects, unintentional incorporation of metal catalyst impurities into silicon nanowires induces a wide range of surface states, particularly on the surfaces at the vicinity of whisker tips, where fortunately the field

strength is at its highest. For instance, localized surface states at the Si(111)/Au interface were identified by Muret using capacitance spectroscopy ranging from  $E_C - 0.35$  eV up to  $E_C$ , having the highest density of  $10^{16}$  cm<sup>-2</sup>eV<sup>-1</sup> at  $E_C - 0.2$  eV [18]. Schmidt et al. demonstrated FI tunneling into these high density states at the interface of *p*-Si(111) and a gold overlay of 3–5 monolayers [19]. As the field was raised, the first line up of the particle ground state took place with the Fermi level of the gold overlay. That is why the field strength obtained in their work was about  $2 \times 10^8$  V/cm, nearly the same as on metals. The surface states close to the conduction band edge came to effect at higher fields. In addition, charging of these high-density states has screened field penetration induced band bending (see Fig. 4 of [19]). Moghal has showed that gold introduces two regions of shallow acceptor surface state energy levels in the silicon band gap at the Si-SiO<sub>2</sub> interface: one at 0.09 eV above  $E_V$  and the other at 0.13 eV below  $E_C$  [20]. The effectiveness of these states in FI process is debatable unless as suggested by Sakurai et al. [21], the electron penetrates the oxide layer. The bulk deep acceptor state of gold which is located 0.54 eV above  $E_V$  can also be effective in FI.

**9) Current-Voltage-Pressure measurements:** Semilog plots of discharge currents recorded using the device made of Sample #1a (undoped whiskers) in N<sub>2</sub> gas versus gas pressure are plotted in Fig. 9a-d. Depending on the bias voltage, various pressure-dependent regimes are observed. Namely, field-ionization (FI) is predominant at pressures in the order of micro-Torr. The rate of field ionization decreases as the pressure increases, as the field-ionization sites are blocked by adsorbed particles. At elevated voltages the curves of  $I$  vs.  $P$  become flat since field-desorption (FD) turns to be the dominant process. Figure 9e shows the  $I$ - $V$  curves obtained from the same device by choosing the sampling pressure (N<sub>2</sub>) randomly (with emphasis at low voltages). At low pressures FI action begins from very low voltages, while at higher pressures ( $\sim 10^{-2}$  Torr), the discharge starts in the ohmic regime and then transfers into field-desorption (FD). The arrow indicates the point at which currents at high pressure exit the quasi-ohmic regime similar to the case of discharge in parallel plate configurations. The ionization currents of N<sub>2</sub> and Ar gases detected by the devices made of Sample #1b (undoped) and Sample #2 (doped whiskers) are plotted in Fig. 9f. These curves along with the curve in the inset of Figure 2f of the manuscript show that the current-pressure dependence is linear at low pressures. The data presented below (Fig. 9) in combination with the curves in Fig. 5 and 6 give a comprehensive perceptive on the dependence of ionization currents upon gas pressure.

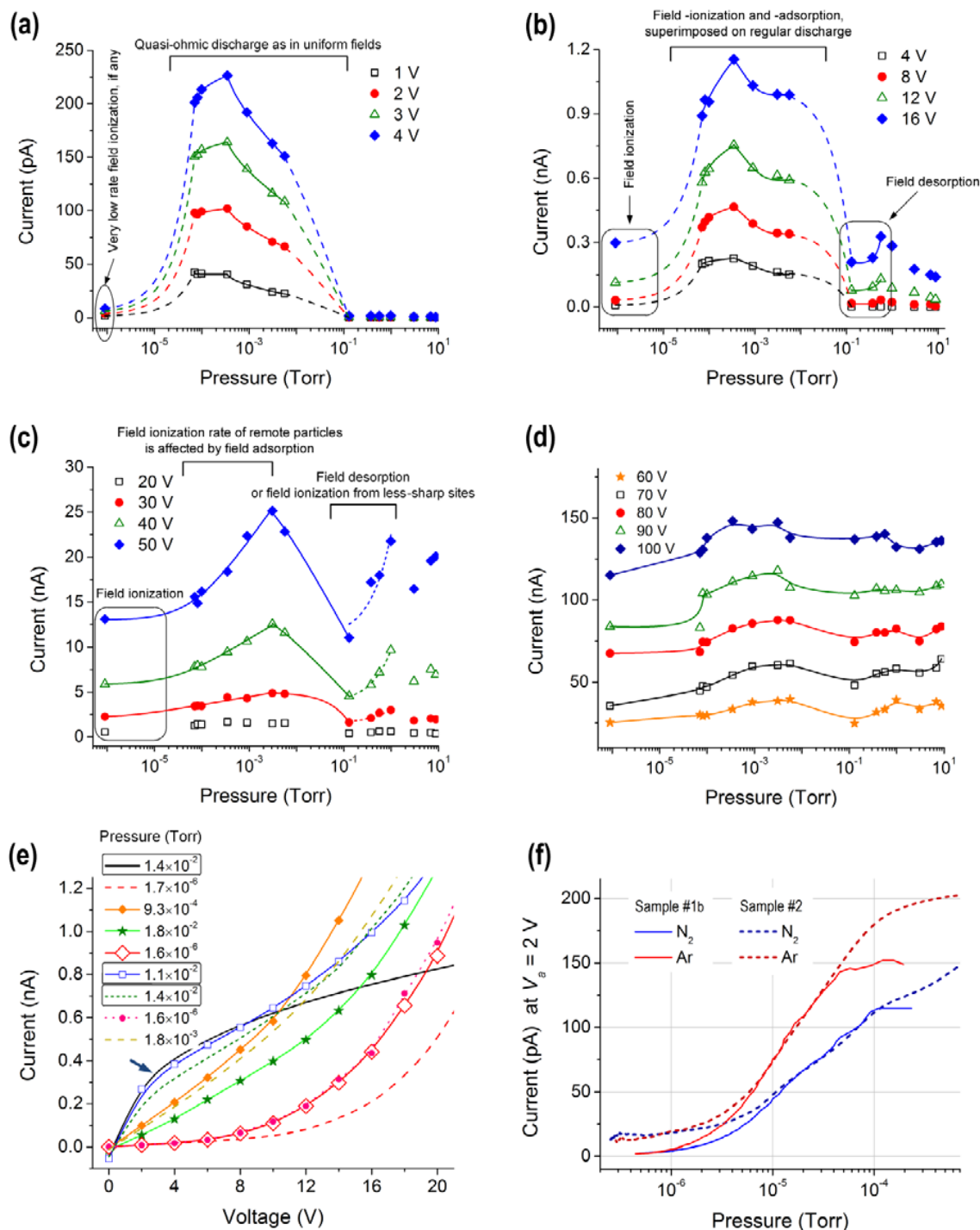


**Fig. 9.** Pressure-Voltage dependence of anomalous ionization currents on whiskered Si nanowires, **a-d)** showing bias dependent regimes, **e)** for  $V_o < 20$  V, and **f)** low pressure discharge currents at a bias of  $V_o = 2$  V for undoped (Sample #1b) and doped (Sample #2) samples. At  $P \lesssim 10^{-5}$  the *p*-type doped sample generates a larger FI current.

## References

- [1] R. G. Forbes, *et al.*, "Some comments on models for field enhancement," *Ultramicroscopy*, vol. 95, pp. 57-65, 2003.
- [2] M. K. Miller, *et al.*, *Atom Probe Field Ion Microscopy*. New York: Oxford, 1996.
- [3] T. T. Tsong, *Atom-Probe Field Ion Microscopy*. Cambridge: Harvard Univ. Press, 1990.
- [4] R. Gomer, *Field emission and field ionization*. Cambridge: Harvard University Press, 1961.
- [5] J. P. Singh, *et al.*, "Field ionization of argon using beta-phase W nanorods," *Applied Physics Letters*, vol. 85, pp. 3226-3228, 2004.
- [6] A. M. Howatson, *An introduction to gas discharges*, 2nd ed. Oxford: Pergamon Press, 1976.
- [7] J. H. Woodruff, *et al.*, "Vertically Oriented Germanium Nanowires Grown from Gold Colloids on Silicon Substrates and Subsequent Gold Removal," *Nano Letters*, vol. 7, pp. 1637-1642, 2007.
- [8] K. K. Lew, *et al.*, "Structural and electrical properties of trimethylboron-doped silicon nanowires," *Applied Physics Letters*, vol. 85, pp. 3101-3103, Oct 2004.
- [9] L. Pan, *et al.*, "Effect of diborane on the microstructure of boron-doped silicon nanowires," *Journal of Crystal Growth*, vol. 277, pp. 428-436, Apr 2005.
- [10] Y. Ohno, *et al.*, "Mechanisms of Field Ionization and Field Evaporation on Semiconductor Surfaces," *Japanese Journal of Applied Physics*, vol. 17, pp. 2013-2022, 1978.
- [11] L. Ernst, "On the field penetration into semiconductors in the field ion microscope," *Surface Science*, vol. 85, pp. 302-308, 1979.
- [12] T. T. Tsong, "Field penetration and band bending near semiconductor surfaces in high electric fields," *Surface Science*, vol. 81, pp. 28-42, 1979.
- [13] K. i. Seo, *et al.*, "Surface Charge Density of Unpassivated and Passivated Metal-Catalyzed Silicon Nanowires," *Electrochemical and Solid-State Letters*, vol. 9, pp. G69-G72, 2006.
- [14] I. Kimukin, *et al.*, "Surface depletion thickness of p-doped silicon nanowires grown using metal-catalysed chemical vapour deposition," *Nanotechnology*, vol. 17, pp. S240-S245, 2006.
- [15] E. C. Garnett, *et al.*, "Dopant profiling and surface analysis of silicon nanowires using capacitance-voltage measurements," *Nat Nano*, vol. 4, pp. 311-314, 2009.
- [16] D. E. Eastman and W. D. Grobman, "Photoemission Densities of Intrinsic Surface States for Si, Ge, and GaAs," *Physical Review Letters*, vol. 28, p. 1378, 1972.
- [17] L. F. Wagner and W. E. Spicer, "Observation of a Band of Silicon Surface States Containing One Electron Per Surface Atom," *Physical Review Letters*, vol. 28, p. 1381, 1972.
- [18] P. Muret, "Capacitance spectroscopy of localized states at metal-semiconductor interfaces. II. Experiments about Ag, Au, and Ni on crystalline (111) Si surfaces," *Journal of Applied Physics*, vol. 53, pp. 6300-6307, 1982.
- [19] W. A. Schmidt, *et al.*, "Field-ion energy spectroscopy of gold overlayers on silicon," *Surface Science*, vol. 194, pp. 127-135, 1988.
- [20] G. R. Moghal, "Investigations of gold surface state energy levels at the silicon-silicon dioxide interface by the MOS capacitance-voltage measurement technique," *Thin Solid Films*, vol. 55, pp. 329-346, 1978.
- [21] T. Sakurai, *et al.*, "Photoillumination effect on silicon field ion microscopy," *Journal of Vacuum Science and Technology*, vol. 16, pp. 626-628, 1979.